Environmental Science & Technology

pubs.acs.org/est

Article

Indoor Air Quality Implications of Germicidal 222 nm Light

Victoria P. Barber,*[,◆] Matthew B. Goss,[◆] Lesly J. Franco Deloya, Lexy N. LeMar, Yaowei Li, Erik Helstrom, Manjula Canagaratna, Frank N. Keutsch, and Jesse H. Kroll*

Cite This: *Environ. Sci. Technol.* 2023, 57, 15990−15998

Read Online

ACCESS | Metrics & More | Article Recommendations | Supporting Information

ABSTRACT: One strategy for mitigating the indoor transmission of airborne pathogens, including the SARS-CoV-2 virus, is irradiation by germicidal UV light (GUV). A particularly promising approach is 222 nm light from KrCl excimer lamps (GUV_{222}); this inactivates airborne pathogens and is thought to be relatively safe for human skin and eye exposure. However, the impact of GUV_{222} on the composition of indoor air has received little experimental study. Here, we conduct laboratory experiments in a 150 L Teflon chamber to examine the formation of secondary species by GUV_{222}. We show that GUV_{222} generates ozone (O_3) and hydroxyl radicals (OH), both of which can react with volatile organic compounds to form oxidized volatile organic compounds and secondary organic aerosol particles. Results are consistent with a box model based on the known photochemistry. We use this model to simulate GUV_{222} irradiation under more realistic indoor air scenarios and demonstrate that under some conditions, GUV_{222} irradiation can lead to levels of O_3, OH, and secondary organic products that are substantially elevated relative to normal indoor conditions. The results suggest that GUV_{222} should be used at low intensities and in concert with ventilation, decreasing levels of airborne pathogens while mitigating the formation of air pollutants.

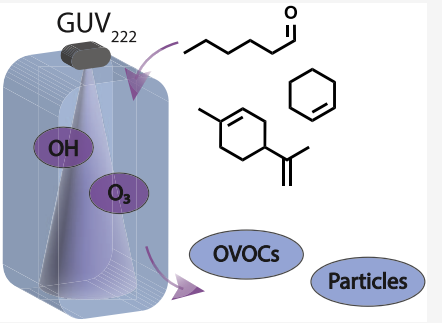

KEYWORDS: *ultraviolet germicidal irradiation, indoor air quality, ozone, photochemistry, ventilation, volatile organic compounds, secondary organic aerosol*

INTRODUCTION

The COVID-19 pandemic has highlighted the critical need to develop and implement strategies to decrease the level of transmission of airborne pathogens. Approaches include both source control (isolation, masking) and remediation (ventilation, air cleaning). One approach that has received substantial attention is the use of germicidal ultraviolet (GUV) light, which inactivates airborne pathogens. This approach goes back decades,[1] traditionally using 254 nm light from mercury lamps. Since light of this wavelength can cause damage to the skin and eyes, care must be taken to minimize occupants' direct exposure to the GUV light.[2,3]

A promising new approach for GUV-based air cleaning is the use of KrCl excimer lamps, which emit at 222 nm (GUV_{222}).[4] In contrast to 254 nm GUV, GUV_{222} does not penetrate deeply into biological materials. Therefore, while GUV_{222} is effective at inactivating airborne viruses and bacteria, it is unable to penetrate the outer layer of dead skin cells or the ocular tear layer.[5] Light at 222 nm is hence less likely to reach and damage living human tissues, offering the potential for air disinfection throughout an occupied indoor space.

A risk with GUV_{222}-based air cleaning, as with all types of air cleaning that rely on chemical and/or photolytic processes, is the potential formation of unwanted secondary byproducts.[6,7] A particular concern with GUV_{222} is the formation of ozone (O_3), a harmful air pollutant that acts as a strong oxidant and can lead to respiratory distress when inhaled.[8] O_3 is formed by the UV photodissociation of oxygen (R1 and R2)

$$O_2 + h\nu_{\lambda<242nm} \rightarrow O + O \quad (1)$$

$$O + O_2 + M \rightarrow O_3 + M \quad (2)$$

Since absorption of UV by O_2, and hence O_3 production, is strongest at short wavelengths,[9] manufacturers of KrCl lamps have added filters to block wavelengths shorter than 222 nm. However, since O_2 absorbs weakly even at 222 nm ($\sigma = 4.09 \times 10^{-24}$ cm^2 [9]), all KrCl lamps have the potential to generate ozone, possibly in concentrations higher than is typically found indoors.[10]

Ozone generated indoors, in addition to posing a direct health hazard, can set off a cascade of chemical reactions that can also affect indoor air quality. Ozone reacts directly with alkenes, present both in the air and on indoor surfaces, forming a range of oxidized volatile organic compounds (OVOCs)[11,12] and secondary organic aerosol (SOA),[13] which may negatively impact human health.[14−17] O_3 chemistry can also lead to the

Received: July 17, 2023
Revised: September 22, 2023
Accepted: September 25, 2023
Published: October 12, 2023

formation of the hydroxyl radical (OH), an even stronger oxidant. This occurs both through reactions with alkenes, which are known to form OH (R3)[11,18] and through O_3 photolysis (R4 and R5).[19]

$$\text{alkene} + O_3 \rightarrow \text{OH} + \text{other products} \quad (3)$$

$$O_3 + h\nu_{\lambda<\sim 370\,\text{nm}} \rightarrow O_2 + O(^1D) \quad (4)$$

$$O(^1D) + H_2O \rightarrow 2\text{OH} \quad (5)$$

Any increased levels of indoor O_3 from GUV_{222} would likely enhance the importance of these reactions, leading to higher levels of indoor OH. This includes O_3 photolysis (R4 and R5), which is the main source of OH in the troposphere; however, under normal conditions, it is negligible in indoor environments due to the lack of low-wavelength UV. Any OH radicals formed from R4 and R5 may then oxidize a wide range of organic species and contribute further to the formation of OVOCs and SOA.

GUV_{222} therefore has the potential to dramatically affect the chemical composition of indoor air and may lead to the formation of chemical species that are hazardous to human health. However, the extent and nature of this impact remain quite uncertain, even as GUV_{222} is being deployed in indoor spaces.[20] Two very recent experimental studies[21,22] demonstrate O_3 production from GUV_{222}, but these do not examine the overall effects on indoor air quality (including the production of OH, OVOCs, and SOA) by GUV_{222}. To the best of our knowledge, the only published work to do so is a box-modeling study by Peng et al.[23] That work predicted that 222 nm irradiation could lead to elevated levels of O_3 and other secondary species relative to nonilluminated conditions, especially under low-ventilation conditions.

Here, we describe a series of laboratory experiments aimed at better understanding the effects of 222 nm irradiation on indoor air quality. The goal of this work is to gain process-based insight into how such irradiation affects the chemical composition of the air; we do not examine the effects of GUV_{222} light on pathogens, indoor surfaces, or human health. These experiments, which use a flow-through Teflon chamber coupled with a range of real-time analytical instruments, explore the effects of several parameters relevant to indoor air processes (VOC level, ventilation, 222 nm light intensity, and humidity) on the generation of oxidants and secondary products. Results are then used to validate a simple chemical model of GUV_{222} irradiation of indoor air, which in turn is used to examine the interplay between GUV_{222} and ventilation in controlling the levels of ozone and other chemical species in the indoor environment.

MATERIALS AND METHODS

Experimental Methods. Experiments are carried out in a 150 L Teflon chamber, outfitted with inlet ports (for introduction of clean air and trace species) and outlet ports (for sampling by analytical instrumentation). Clean dry air from a zero-air generator (Aadco Model 737) is introduced into the chamber either directly or after passing through a bubbler filled with Milli-Q water. Mass flow controllers are used to adjust these two flows to control the chamber's relative humidity. Dilution rates are measured using acetonitrile, an inert dilution tracer ($k_{dilution}$ = 8.0 × 10^{-4} to 9.7 × 10^{-4} s^{-1}, 2.9−3.5 ACH). Most experiments are conducted at 22 °C and ∼25% RH, while "higher RH" experiments are carried out at ∼45% RH.

GUV_{222} light is provided by a single filtered KrCl excimer lamp (Ushio, Care222 B1 Illuminator, peak emission at 222 nm), centered directly above the Teflon chamber. The average fluence rate within the chamber is ∼45 $\mu W/cm^2$, estimated geometrically from the lamp intensity profile provided by the manufacturer[24] (see Section S1.1). The indirect estimation of the lamp intensity is a limitation of this work, but the agreement between modeled and measured ozone production (see Results and Discussion Section) indicates that it is reasonably accurate. More quantitative estimates of UV fluence rate and its relationship to O_3 generation are available in recent work by Peng et al.[22] and Link et al.[21] Most experiments are carried out at full light intensity. For "low-light" experiments, the lamp emission is attenuated by several layers of plastic, achieving a factor of ∼5 reduction in intensity (determined by the reduction in the steady-state O_3 concentration, which is assumed to scale linearly with average UV fluence).[21,22] For the "O_3-only" experiments, the light is left off, and O_3 is introduced via a Pen-Ray ozone generator, with a steady-state O_3 concentration matching that of the GUV_{222} experiments (∼100 ppb). Reaction conditions for each experiment are described in detail in Table S1.

For all VOC oxidation experiments, the chamber is first allowed to reach a steady-state concentration of O_3, via either 222 nm irradiation or direct addition. This is followed by the addition of 5.3 ppb of acetonitrile (the dilution tracer) (C_2H_3N, 99.8%, Sigma-Aldrich), 1.2 ppb of 1-butan-d9-ol (intended as an OH tracer, but not used here due to the relatively low OH levels) (C_4D_9OH, 98%, Cambridge Isotope Laboratories, Inc.), and 120 ± 11 $\mu g\ m^{-3}$ of ammonium sulfate particles (to act as seed particles for any SOA production) ($(NH_4)_2SO_4$, ≥99%, Sigma-Aldrich). Finally, the relevant VOC (10 or 100 ppb) is added to the chamber. VOCs used in this study include hexanal ($C_6H_{12}O$, 98%, Sigma-Aldrich), cyclohexene (C_6H_{10}, 99%, Sigma-Aldrich), and (*R*)-(+)-limonene ($C_{10}H_{16}$, 97%, Sigma-Aldrich). Reactant addition procedures are described in greater detail in Section S1.2. Because the oxidants are already present in the chamber, oxidation begins immediately, so VOC injection is taken as t = 0.

Real-time measurements of gas- and particle-phase composition in the chamber are conducted using a suite of analytical instruments. Ozone is measured by a UV absorption monitor (2BTech). NO_x is monitored using a chemiluminescence NO−NO_2−NO_X analyzer (Thermo Fisher Scientific) and was below the instrument detection limit in all experiments. Reactant VOC and OVOC products are monitored using a Vocus proton transfer reaction mass spectrometer (PTR-MS, Tofwerk, Aerodyne Research, Inc.[25]) and an ammonium chemical ionization mass spectrometer (NH_4^+ CIMS, modified PTR3, see Zaytsev et al.[26]). Particle concentration and composition are measured using a scanning mobility particle sizer (SMPS, TSI) and an aerosol mass spectrometer (AMS, Aerodyne Research, Inc.[27]). Analytical instruments are summarized in Table S2. Gas-phase mass spectrometric data are background-subtracted and corrected for dilution. The analysis does not account for variations in detection efficiencies, which may be substantial;[26] therefore, we report relative signals, which are unaffected by such calibration uncertainties, rather than absolute concentrations. Particle-phase data are corrected for dilution and wall losses by

https://doi.org/10.1021/acs.est.3c05680
Environ. Sci. Technol. 2023, 57, 15990−15998

normalizing to the ammonium sulfate seed particle concentration. Data analysis and quantification approaches are described in more detail in Section S1.3.

RESULTS AND DISCUSSION

Ozone Production. The production of ozone by 222 nm light is examined via the irradiation of clean chamber air. Figure 1 shows results from four representative irradiation

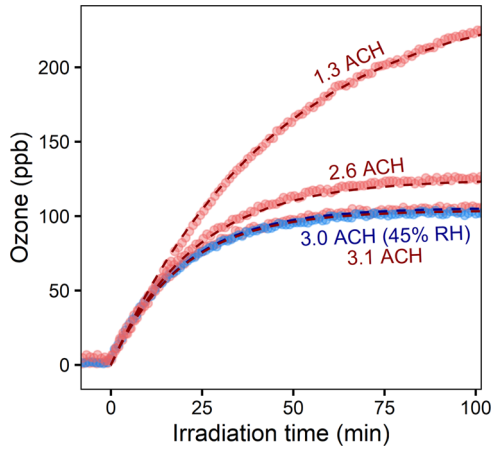

Figure 1. Observed ozone production for clean-chamber irradiation experiments. Measurements agree well with the predictions from the simple box model (dashed lines) across a range of ventilation rates and relative humidities. Measurements shown in red are taken at 25% RH.

experiments, run at different ventilation rates (1.3−3.1 air changes per hour (ACH)) and relative humidities (25−45%). O_3 production is observed to occur immediately when the lights are turned on. O_3 levels increase quickly at first, eventually leveling off to a steady-state value, in which photolytic production is balanced by removal by outflow. The O_3 production rate is measured at 324 ± 18 ppb h^{-1}, in reasonably good agreement with previous measurements[22] when differences in average GUV_{222} fluence rate are considered (see Section S3.1). The steady-state O_3 concentration is independent of relative humidity and inversely proportional to the ventilation rate (Figure S3).

Dashed lines in Figure 1 denote the O_3 concentrations predicted from a simple box model. This model includes O_2 photolysis (R1 and R2), O_x−HO_x chemistry, and dilution (see Table S3 for rate constants and photochemical parameters[9−11,28−32]). Model parameters (e.g., light intensity, air-exchange rate, and RH) are matched to each experiment. O_3 deposition, which is likely small on Teflon surfaces, is not included. The model accurately predicts measured O_3 levels, indicating that the processes describing ozone levels (formation from O_3 photolysis at 222 nm and loss by outflow) are well-captured by the simple model.

Decay of VOCs upon 222 nm Irradiation. In a second set of experiments (Table S1), VOCs are added to the irradiated chamber after the O_3 levels reach a steady state. Experiments center on two VOCs: hexanal, a C6 compound that reacts only with OH, and cyclohexene, a C6 compound that reacts with both OH and O_3. VOC decays are shown in Figure 2. Negligible change in the O_3 concentration is observed upon introduction of 10 ppb of VOC; when 100 ppb of cyclohexene is introduced, a small O_3 depletion (~4.3 ppb) is observed.

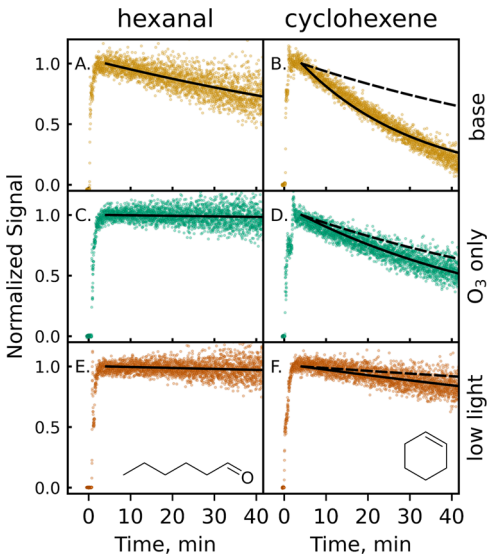

Figure 2. Normalized decays of two VOCs (hexanal and cyclohexene) after introduction to the GUV_{222}-irradiated chamber (see also Figure S4). Time = 0 refers to when the VOC was injected into the chamber. Traces are background- and dilution-corrected, so observed decays are from oxidative loss only. Details of each experimental condition (base, O_3 only, low light) are given in the text and Table S1. Solid black lines denote single-exponential fits to the observed decays; dashed black lines show the expected decay of cyclohexene from reaction with O_3 only.[28]

Under "base conditions" (10 ppb VOC precursor, 222 nm light, ~25% RH) (Figure 2AB), the concentrations of both hexanal and cyclohexene decrease after being introduced into the irradiated chamber. Concentrations are corrected for dilution; losses by direct photolysis and uptake to surfaces are expected to be minimal (Section S3.2). Therefore, decays indicate oxidative loss only. This oxidation cannot be explained by O_3 alone. Hexanal does not react with O_3− a very small decay of hexanal is attributed to minor, nonoxidative loss pathways (see SI). While cyclohexene does react with O_3, its decay is far faster than what can be attributed to the O_3 reaction (dashed line). Indeed, for experiments in which the GUV_{222} light is off and VOCs are exposed to the same levels of O_3 as in the irradiated case (Figure 2CD), the hexanal does not decrease at all, and cyclohexene decays far less than in the irradiation case, at a rate consistent with the reaction with O_3 (plus a small contribution from OH generated by the ozonolysis reaction, reaction R3). This observed "excess reactivity" (the difference in observed decays and decays expected from the O_3 reaction alone) indicates that GUV_{222} irradiation generates not only O_3 but other oxidants as well.

Additional experiments carried out under a range of reaction conditions provide evidence that these additional oxidants are OH radicals, formed from reactions R3−R5. For example, experiments with the 222 nm fluence rate attenuated substantially (~9 μW cm^{-2}, Figure 2EF) exhibit VOC decay rates that are much slower compared to those under base conditions. This attenuation is assumed to decrease steady-state O_3 concentrations proportionally. However, the observed excess reactivity disproportionately decreases by approximately an order of magnitude. This is consistent with OH formation,

https://doi.org/10.1021/acs.est.3c05680
Environ. Sci. Technol. 2023, 57, 15990−15998

which depends on the photolysis of both O_2 and O_3, as well as (in the case of cyclohexene) the ozonolysis reaction. The dependence of decay on other experimental parameters, such as VOC concentration and relative humidity, are also consistent with OH production from GUV_{222} lights; this is discussed in detail in Section S3.3.

We estimate the average OH levels in all experiments using an exponential fit to the VOC time series and known OH rate constants.[29,30] For cyclohexene experiments, the average measured [O_3] and the O_3 + cyclohexene rate constant are included in the fit to account for excess reactivity. The range of [OH] measured in each experiment is calculated by applying the same exponential fits to a rolling 15 min window (see Section S3.4 for more details). We also calculate OH levels using our simple box model by including a highly simplified oxidation scheme (Table S3) for each injected VOC. Reaction rates of the VOC with OH and O_3 are taken from the literature, and the oxidation products are assumed to have the same OH reactivities as their precursors. Measured and modeled average [OH] agree well (Figure 3), providing

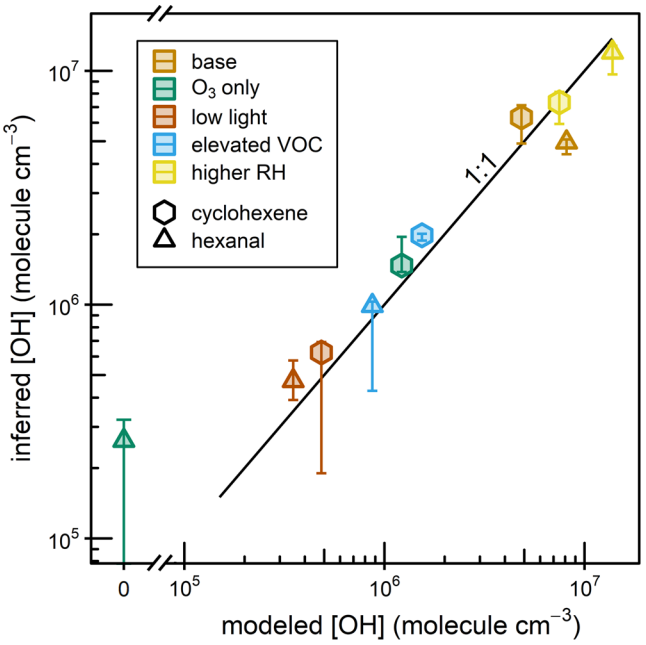

Figure 3. Experimentally derived average OH concentration vs average OH concentration predicted by the box model for all cyclohexene and hexanal experiments (see Section S3.4). Note the break in the *x*-axis. Error bars represent the range of values observed throughout the experiment.

strong evidence that GUV_{222} produces not only O_3 (R1 and R2) but also OH (R3 and R5), and that oxidation by both O_3 and OH can take place upon irradiation with 222 nm light.

Formation of Gas-Phase Oxidation Products. The formation of oxidized gas-phase products is observed in all experiments in which VOC oxidation occurs. Product distributions for three cyclohexene experiments (base conditions, O_3 only, and low light) are shown in Figure 4. Additional product distributions and time series results (including for the hexanal experiments) are provided in Figures S5 and S6.

Measured products are dominated by C6 and C5 compounds, as expected, given that cyclohexene is a C6 species. The two products with the largest mass spectrometric signals, $C_6H_{10}O_2$ and $C_6H_{10}O_3$, are the major products of the OH- and O_3-initiated oxidation of cyclohexene, respectively[33,34] (see Scheme S1) (products are detected as the analyte-NH_4^+ adduct, and reported as the analyte formula.) The ratios of the signals from the two products vary among experiments, indicating differences in the relative concentrations of OH and O_3. In Figure 4b, the ratio of the mass spectrometric signals of these two products is shown vs the relative OH-to-O_3 oxidation rate ratios (calculated from the experimentally determined values of [OH] and [O_3]) for each cyclohexene experiment. A strong correlation (R^2 = 0.98) is found between the two ratios, providing further support for OH-initiated oxidation and more generally for OH radical production from irradiation by 222 nm light. The products formed in the 222 nm irradiation of hexanal are also broadly consistent with OH-initiated oxidation (see Scheme S2).[35]

Secondary Organic Aerosol Formation. In all experiments, dry ammonium sulfate seed particles are added to the chamber, providing surface area onto which low-volatility species may condense and enabling the assessment of potential SOA formation. SOA formation is observed in a number of experiments (Table S1 and Figure S7). SOA formation is generally modest for most hexanal and cyclohexene experiments, likely due to the relatively small size (C6) and low concentrations (10 ppb) of those species. Higher concentrations of SOA are observed for experiments with high initial concentrations (100 ppb) of hexanal or cyclohexene and for those using limonene ($C_{10}H_{16}$, a monoterpene commonly found in fragrances and cleaning products). In fact, the GUV_{222} irradiation of 100 ppb limonene (a level that can be found in indoor environments immediately after cleaning events[36,37]) results in exceedingly high SOA loadings, on the order of 400 ± 80 μg m.$^{-3}$ Additionally, new particle formation is observed upon 222 nm irradiation under some conditions (Section S3.6 and Figure S8). This effect is not observed when the corresponding amount of O_3 is added without 222 nm irradiation. GUV_{222}-induced nucleation occurs even when no VOCs are added and so may result from photochemistry of organic species on the chamber surfaces, or even of the surface materials themselves. Whether this is a general feature of the irradiation of organics on indoor surfaces is unclear from the present experiments, but it does suggest that 222 nm irradiation may induce new particle formation in some environments.

Extrapolation to Indoor Environments. The above laboratory experiments demonstrate that GUV_{222} irradiation forms ozone, OH, and a range of oxidation products, measured ozone and inferred OH agree broadly with predictions from a photochemical box model. However, real-world indoor environments are substantially different than our simple laboratory system: they involve a large number of organic compounds, depositional loss of ozone and other species, infiltration of outdoor pollutants, a wide range of possible ventilation rates, and typically much lower average UV fluence rates. Here, we extend our photochemical model to a more realistic indoor air scenario with the goal of understanding how GUV_{222} may impact indoor air quality under a range of ventilation and irradiation conditions.

For simulations of chemistry in a more realistic indoor environment, two "lumped" VOCs are included in the model: one (VOC1) that reacts with OH but not with O_3 and another (VOC2) that reacts with both OH and O_3. Rate constants for VOC1 are chosen based on typical values for indoor VOCs

https://doi.org/10.1021/acs.est.3c05680
Environ. Sci. Technol. 2023, 57, 15990−15998

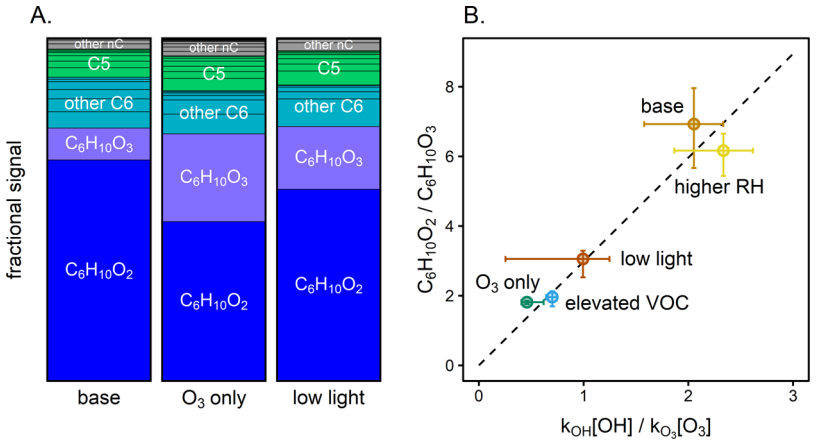

Figure 4. Gas-phase products from cyclohexene experiments. Panel A: Normalized mass spectrometric signal of products formed in the GUV_{222} irradiation (base conditions), O_3-only, and low-light experiments (see Section S3.5 for calculations and Figure S5 for other experimental conditions). Signals are integrated from t = 250−2500 s, normalized to the total integrated ion signal, and grouped by carbon number (nC). In all cases, products are dominated by $C_6H_{10}O_2$ (the major cyclohexene + OH reaction product) and $C_6H_{10}O_3$ (the major cyclohexene + O_3 product). Panel B: The ratio of the $C_6H_{10}O_2$-to-$C_6H_{10}O_3$ signals vs the ratio of the rates of OH and O_3 oxidation, for all cyclohexene experiments. Concentrations of OH are determined from the fits in Figure 2, while concentrations of O_3 are measured directly. The dashed line is a linear fit to the data; since the two products have differing sensitivities in the instrument, this differs from the 1:1 line. Error bars represent the range of values observed throughout the experiment.

(Section S2.1 and Tables S3 and S4); rate constants for VOC2 are assumed to be equal to those of limonene. OH yields from O_3 + VOC2 are assumed to be 0.86, equal to that of limonene.[11] All oxidation reactions form lumped organic products that can also react with OH. VOC emission rates (84 ppb h^{-1} and 4.2 ppb h^{-1} for VOC1 and VOC2, respectively) are determined from previous measurements of OH and O_3 reactivities in indoor environments;[38,39] details of these calculations are given in Section S2.1. The model is run at 298 K, 1 atm, and 30% RH. We also include a background concentration of O_3 in the ventilation air (40 ppb, consistent with typical outdoor O_3 concentrations), a 25% loss of O_3 to the ventilation system, and an O_3 deposition constant of 3 h^{-1}.[10,31]

The range of light fluence rates chosen covers the US and international guidelines on 222 nm exposure limits (ranging from 0.8 to 16 $\mu W/cm^2$ assuming a continuous 8 h exposure[40,41]) as well as the values in previous studies used for pathogen deactivation (average irradiance of up to 2.73 $\mu W/cm^2$ at 1.7 m above the ground from Eadie et al.[42] and 3.5 $\mu W/cm^2$ from Peng et al.[23]). The range used in our model extends higher to take into account proposals for the use of significantly higher light fluence rates,[43] and include the fluence rates in our experiments (~45 $\mu W/cm^2$). Ventilation rates span a range of typical indoor values and include the minimum American Society of Heating, Refrigerating and Air-Conditioning Engineers (ASHRAE) recommendations for homes (0.35 ACH), offices (~2−3 ACH), and healthcare settings (10 ACH).[44]

Key model results are shown in Figure 5. Figure 5A shows the effective air change rate (eACH) across a wide range of GUV_{222} fluence and ventilation rates; even modest irradiation levels lead to substantial increases in eACH (see also Figure S9A). Figure 5B−D shows the steady-state indoor concentrations of O_3, OH, and total oxidation products (assuming unit yield), respectively.

Steady-state ozone levels (Figure 5B) are higher with 222 nm irradiation than without. Sources of O_3 include photochemistry (R1 and R2) and infiltration of outdoor air, while sinks include deposition, ventilation, and chemical reaction (rates and contributions of individual processes are given in Figure S9B−E). With low irradiation, the O_3 levels are governed mainly by infiltration of outdoor air, and the O_3 increases are modest. Under the highest fluence rates (>25 $\mu W/cm^2$), and especially under low ventilation rates (<1 ACH), indoor O_3 can reach levels exceeding that of the outdoors and can even exceed the OSHA indoor limit of 100 ppb. However, even a small change in indoor O_3 levels can have a dramatic effect on people's total ozone exposure,[46] given the large fraction of time people spend indoors. In most cases, deposition represents the dominant sink of ozone (Figure S9D).

Figure 5C shows steady-state levels of OH as a function of ventilation and 222 nm light intensity. Sources of OH include O_3-alkene reactions (R3) and photochemistry (R4 and R5), while sinks are dominated by reactive losses (see also Figure S9F,G). In the absence of GUV_{222} irradiation, modeled OH is from alkene ozonolysis only, with predicted levels (~10^5 molecules cm^{-3}) overlapping but falling on the low end of the measured and modeled OH in indoor spaces (which range from 6 × 10^4 to 1.6 × 10^6 molecules cm^{-3});[47−56] this underestimation may arise from the omission of photolysis of trace species such as nitrous acid (HONO) or aldehydes, which may be important in some environments.[57] As is the case for O_3, GUV_{222} irradiation leads to increases in indoor levels of OH. At low to moderate irradiation levels, this increase in OH is mostly due to the alkene ozonolysis reaction; however, at higher levels, ozone photolysis plays a larger role (Figure S9G). OH increases with increasing photochemistry (higher GUV_{222} fluence rates and ozone concentrations) but is substantially modulated by losses from reaction with VOCs. VOC concentrations are higher at low ventilation rates (Figure S9H) due to the buildup of emitted VOCs, which suppresses the OH concentrations. At high light intensities, steady-state OH levels can approach outdoor levels, matching or exceeding indoor OH measurements during transient events such as cleaning or cooking activities.[58,59]

https://doi.org/10.1021/acs.est.3c05680
Environ. Sci. Technol. 2023, 57, 15990−15998

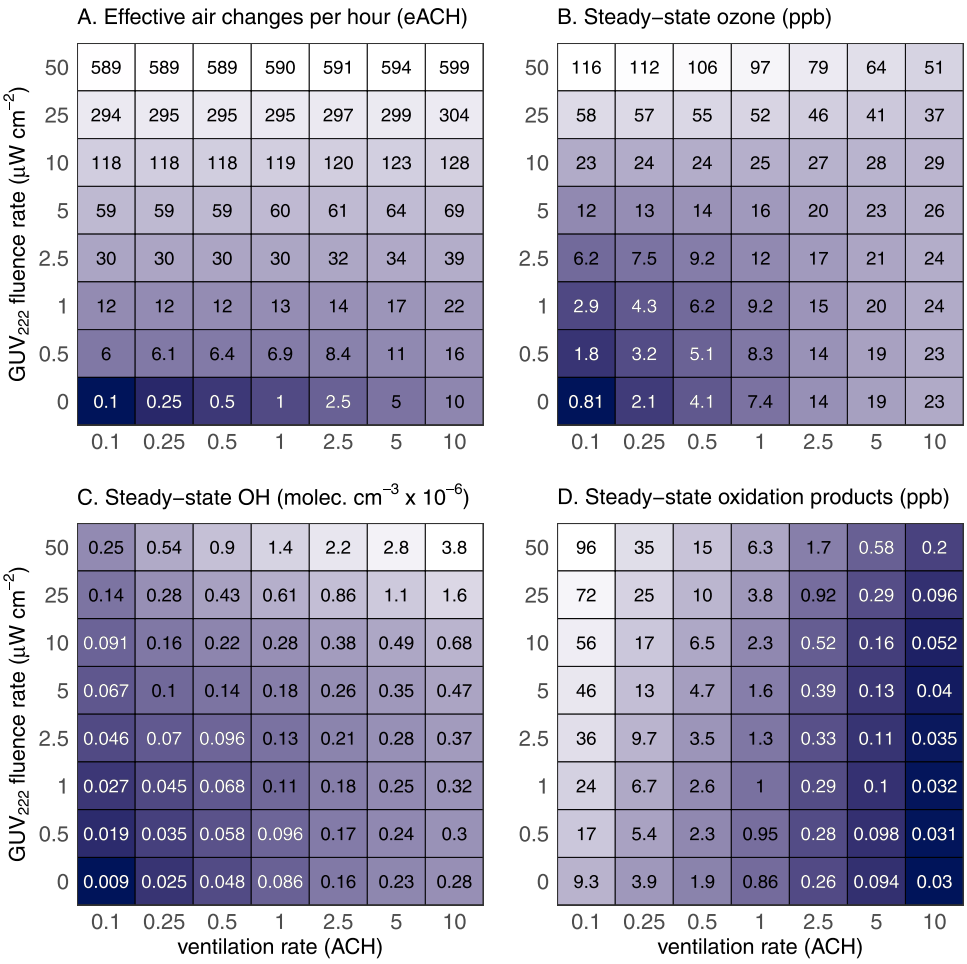

Figure 5. Effects of ventilation and GUV_{222} fluence rate on modeled GUV efficacy and indoor air quality (see also Figures S9−S12). Panel A: effective air changes per hour (eACH) for indoor pathogens, based on the previously reported inactivation rate of SARS-CoV-2 at 222 nm[45] (Section S4.2). Panels B−D: steady-state concentrations of (B) O_3, (C) OH, and (D) organic oxidation products, respectively, as predicted by the photochemical box model. Panel D calculations assume unit yields and do not account for VOC production from surfaces (see Figure S11) or recycling by NO_x−HO_x interactions (Figure S12), so they likely represent lower limits. Lighter colors represent larger values; note that the logarithmic color scaling is different for each panel. Additional model results are given in Figures S9 and S10.

The production of O_3 and OH by GUV_{222}-driven chemistry and their subsequent reactions with VOCs lead to an increase in organic oxidation products (OVOCs and SOA). Steady-state levels and production rates of such products (assuming unit yields) are listed in Figures 5D and S9I. Concentrations increase with increased light intensity and are especially high at low ventilation rates. Since more than one product molecule may be formed per oxidation reaction and OVOCs may also be formed by surface reactions of O_3 or OH, these numbers likely represent lower limits. Of particular concern are hazardous air pollutants (HAPs, such as CH_2O) and SOA, both of which may represent health hazards in the indoor environment. Concentrations of SOA are challenging to predict, as SOA production depends on the amounts and identity of the indoor VOCs, as well as on a host of reaction conditions. However, SOA levels on the order of a few $\mu g/m^3$ might occur (Figure S10); the production of SOA from 222 nm irradiation in realistic indoor settings is an important area of future research.

The simplicity of the model neglects some additional secondary effects, which are highly uncertain. For example, volatile secondary organic products stemming from reactive surface losses of O_3 (e.g., to paint, textiles, skin)[12,60] could represent an additional secondary effect of GUV_{222} on indoor air quality. Preliminary modeling suggests that this may increase OVOC concentrations by as much as a factor of 100 (Figure S11). Similarly, indoor environments contain NO_X, which can affect the levels and fates of oxidants. While NO_X chemistry is not modeled explicitly here, due in part to uncertainties in NO_X photolysis processes, we carried out additional simulations to estimate the role of HOx-NO_X cycling. As shown in Section S4.1 and Figure S12, such cycling substantially increases OH concentrations and OVOC product formation. We do not examine the role of HONO, which can be present in high (ppb) levels indoors[55] and absorbs strongly at 222 nm ($\sigma = 1.35 \times 10^{-18}$ cm^2[29]); HONO photolysis may lead to even higher OH levels than predicted here. All of these effects have the potential to increase OVOC formation, suggesting that the OVOC concentrations presented in Figure 5 are best understood as a lower limit and that the indoor air quality impacts of 222 nm irradiation could be more severe than those predicted here.

Implications. Our laboratory studies demonstrate that GUV_{222} light leads to the production of (1) ozone, (2) OH radicals, and (3) secondary organic species (OVOCs and SOA); these are in broad agreement with prior model predictions.[23] The resulting concentrations of such secondary

https://doi.org/10.1021/acs.est.3c05680
Environ. Sci. Technol. 2023, 57, 15990−15998

species can be substantially higher than those normally found in indoor environments; in extreme cases, these increases can be dramatic, leading to oxidation conditions similar to those found in the outdoors during daytime hours. The negative health impacts associated with the unavoidable generation of these secondary species, most importantly O_3, fine particular matter, and HAPs, thus need to be taken into account (and ideally mitigated) when considering the use of 222 nm disinfection in indoor spaces.

While a detailed analysis of the health impacts of GUV_{222} use (both the benefits from the inactivation of airborne pathogens and the drawbacks from secondary pollutant formation) is beyond the scope of this work, our results offer some broad guidance as to the optimal use of GUV_{222} in indoor environments. Most importantly, GUV_{222} disinfection alone is not a safe substitute for ventilation as a means to control levels of indoor airborne pathogens, as it can lead to the buildup of indoor ozone and other pollutants to dangerous levels (Figure 5). However, GUV_{222} may be effectively used in conjunction with ventilation: relatively modest irradiation levels combined with carefully chosen ventilation conditions can greatly enhance the effective air change rate (Figure 5A) while limiting the levels of secondary pollutants (Figure 5B–D). Moreover, due to the unavoidable formation of secondary pollutants, GUV_{222} lights should be run at the lowest effective levels whenever possible. Further, the combination of GUV_{222} irradiation with air-cleaning technologies (e.g., sorbents for ozone and OVOCs, filters for particulate matter) may serve to minimize indoor secondary pollutant levels, potentially enabling safer use of GUV_{222} under poorly ventilated environments. Quantifying the benefits and trade-offs of these combined approaches (ventilation, GUV_{222} irradiation, and/or air cleaning) in terms of pathogen transmission, air pollutant levels, human health, and cost-effectiveness is a critical next step toward ensuring healthier indoor environments.

■ ASSOCIATED CONTENT

Supporting Information

The Supporting Information is available free of charge at https://pubs.acs.org/doi/10.1021/acs.est.3c05680.

Experimental conditions and methods; additional modeling methods; additional results and discussion (including ozone steady-state calculations; discussion of VOC loss pathways; discussion of elevated VOC and RH experiments; more complete product distribution figures; reaction schemes; and SMPS data); model results (including additional model output figures and calculation of effective air changes per hour) (PDF)

■ AUTHOR INFORMATION

Corresponding Authors

Victoria P. Barber − *Department of Civil and Environmental Engineering, Massachusetts Institute of Technology, Cambridge, Massachusetts 02139, United States;* Present Address: Department of Chemistry and Biochemistry, University of California Los Angeles, Los Angeles, California 90095, United States; orcid.org/0000-0003-4543-4657; Phone: 424-259-5198.; Email: vbarber@chem.ucla.edu

Jesse H. Kroll − *Department of Civil and Environmental Engineering, Massachusetts Institute of Technology, Cambridge, Massachusetts 02139, United States; Department of Chemical Engineering, Massachusetts Institute of Technology, Cambridge, Massachusetts 02139, United States;* orcid.org/0000-0002-6275-521X; Phone: 617-253-2409; Email: jhkroll@mit.edu

Authors

Matthew B. Goss − *Department of Civil and Environmental Engineering, Massachusetts Institute of Technology, Cambridge, Massachusetts 02139, United States*

Lesly J. Franco Deloya − *Department of Earth, Atmospheric, and Planetary Sciences, Massachusetts Institute of Technology, Cambridge, Massachusetts 02139, United States*

Lexy N. LeMar − *Department of Chemical Engineering, Massachusetts Institute of Technology, Cambridge, Massachusetts 02139, United States*

Yaowei Li − *John A. Paulson School of Engineering and Applied Sciences, Harvard University, Cambridge, Massachusetts 02138, United States;* orcid.org/0000-0003-0725-6108

Erik Helstrom − *Department of Civil and Environmental Engineering, Massachusetts Institute of Technology, Cambridge, Massachusetts 02139, United States*

Manjula Canagaratna − *Center for Aerosol and Cloud Chemistry, Aerodyne Research Incorporated, Billerica, Massachusetts 01821, United States*

Frank N. Keutsch − *John A. Paulson School of Engineering and Applied Sciences, Harvard University, Cambridge, Massachusetts 02138, United States; Department of Chemistry and Chemical Biology and Department of Earth and Planetary Sciences, Harvard University, Cambridge, Massachusetts 02138, United States*

Complete contact information is available at: https://pubs.acs.org/10.1021/acs.est.3c05680

Author Contributions

◆V.P.B. and M.B.G. contributed equally to this work.

Notes

The authors declare no competing financial interest.

■ ACKNOWLEDGMENTS

This work is supported by the U.S. National Science Foundation under grants ECS-2108811 and AGS-2129835 and the Harvard Global Institute. M.B.G. is supported by NIEHS Toxicology Training Grant #T32-ES007020. The authors thank Bella Nesti (Harvard University) for assisting with the initial phases of data analysis, and Jose Jimenez (University of Colorado Boulder), Aaron Collins (Open-Aeros), and Holger Claus (Ushio Inc.) for helpful discussions.

■ REFERENCES

(1) Wells, W. F.; Wells, M. W.; Wilder, T. S. The Environmental Control of Epidemic Contagion: I. An Epidemiologic Study of Radiant Disinfection of Air in Day Schools. *Am. J. Epidemiol.* **1942**, *35* (1), 97−121.

(2) Nardell, E. A. Air Disinfection for Airborne Infection Control with a Focus on COVID-19: Why Germicidal UV Is Essential. *Photochem. Photobiol.* **2021**, *97* (3), 493−497.

(3) Centers for Disease Control and Prevention. Upper Room Ultraviolet Germicidal Irradiation (UVGI). https://www.cdc.gov/coronavirus/2019-ncov/community/ventilation/uvgi.html (accessed May 17, 2023).

(4) Blatchley, E. R.; Brenner, D.; Claus, H.; Cowan, T. E.; Linden, K.; Liu, Y.; Mao, T.; Park, S.-J.; Simons, R.; Sliney, D. *Far UV-C*

Radiation: Current State-of Knowledge, International Ultraviolet Association Task Force.
(5) Buonanno, M.; Welch, D.; Shuryak, I.; Brenner, D. J. Far-UVC Light (222 Nm) Efficiently and Safely Inactivates Airborne Human Coronaviruses. *Sci. Rep.* **2020**, *10* (1), No. 10285.
(6) Collins, D. B.; Farmer, D. K. Unintended Consequences of Air Cleaning Chemistry. *Environ. Sci. Technol.* **2021**, *55* (18), 12172−12179.
(7) Ye, Q.; Krechmer, J. E.; Shutter, J. D.; Barber, V. P.; Li, Y.; Helstrom, E.; Franco, L. J.; Cox, J. L.; Hrdina, A. I. H.; Goss, M. B.; Tahsini, N.; Canagaratna, M.; Keutsch, F. N.; Kroll, J. H. Real-Time Laboratory Measurements of VOC Emissions, Removal Rates, and Byproduct Formation from Consumer-Grade Oxidation-Based Air Cleaners. *Environ. Sci. Technol. Lett.* **2021**, *8* (12), 1020−1025.
(8) Turner, M. C.; Jerrett, M.; Pope, C. A.; Krewski, D.; Gapstur, S. M.; Diver, W. R.; Beckerman, B. S.; Marshall, J. D.; Su, J.; Crouse, D. L.; Burnett, R. T. Long-Term Ozone Exposure and Mortality in a Large Prospective Study. *Am. J. Respir. Crit. Care Med.* **2016**, *193* (10), 1134−1142.
(9) J. B. Burkholder, S. P. Sander, J. Abbatt, J. R. Barker, C. Cappa, J. D. Crounse, T. S. Dibble, R. E. Huie, C. E. Kolb, M. J. Kurylo, V. L. Orkin, C. J. Percival, D. M. Wilmouth, and P. H. Wine *Chemical Kinetics and Photochemical Data for Use in Atmospheric Studies, Evaluation No. 19*, JPL Publication 19-5, Jet Propulsion Laboratory, Pasadena, 2019http://jpldataeval.jpl.nasa.gov.
(10) Nazaroff, W. W.; Weschler, C. J. Indoor Ozone: Concentrations and Influencing Factors. *Indoor Air* **2022**, *32* (1), No. e12942.
(11) Calvert, J. G. *The Mechanisms of Atmospheric Oxidation of the Alkenes*; Oxford University Press, 2000.
(12) Wisthaler, A.; Weschler, C. J. Reactions of Ozone with Human Skin Lipids: Sources of Carbonyls, Dicarbonyls, and Hydroxycarbonyls in Indoor Air. *Proc. Natl. Acad. Sci. U.S.A.* **2010**, *107* (15), 6568−6575.
(13) Kroll, J. H.; Seinfeld, J. H. Chemistry of Secondary Organic Aerosol: Formation and Evolution of Low-Volatility Organics in the Atmosphere. *Atmos. Environ.* **2008**, *42* (16), 3593−3624.
(14) US EPA. Dose-Response Assessment for Assessing Health Risks Associated with Exposure to Hazardous Air Pollutants. https://www.epa.gov/fera/dose-response-assessment-assessing-health-risks-associated-exposure-hazardous-air-pollutants (accessed May 02, 2023).
(15) Dockery, D. W.; Pope, C. A.; Xu, X.; Spengler, J. D.; Ware, J. H.; Fay, M. E.; Ferris, B. G.; Speizer, F. E. An Association between Air Pollution and Mortality in Six U.S. Cities. *N. Engl. J. Med.* **1993**, *329* (24), 1753−1759.
(16) Burnett, R.; Chen, H.; Szyszkowicz, M.; Fann, N.; Hubbell, B.; Pope, C. A.; Apte, J. S.; Brauer, M.; Cohen, A.; Weichenthal, S.; Coggins, J.; Di, Q.; Brunekreef, B.; Frostad, J.; Lim, S. S.; Kan, H.; Walker, K. D.; Thurston, G. D.; Hayes, R. B.; Lim, C. C.; Turner, M. C.; Jerrett, M.; Krewski, D.; Gapstur, S. M.; Diver, W. R.; Ostro, B.; Goldberg, D.; Crouse, D. L.; Martin, R. V.; Peters, P.; Pinault, L.; Tjepkema, M.; van Donkelaar, A.; Villeneuve, P. J.; Miller, A. B.; Yin, P.; Zhou, M.; Wang, L.; Janssen, N. A. H.; Marra, M.; Atkinson, R. W.; Tsang, H.; Quoc Thach, T.; Cannon, J. B.; Allen, R. T.; Hart, J. E.; Laden, F.; Cesaroni, G.; Forastiere, F.; Weinmayr, G.; Jaensch, A.; Nagel, G.; Concin, H.; Spadaro, J. V. Global Estimates of Mortality Associated with Long-Term Exposure to Outdoor Fine Particulate Matter. *Proc. Natl. Acad. Sci. U.S.A.* **2018**, *115* (38), 9592−9597.
(17) Pye, H. O. T.; Ward-Caviness, C. K.; Murphy, B. N.; Appel, K. W.; Seltzer, K. M. Secondary Organic Aerosol Association with Cardiorespiratory Disease Mortality in the United States. *Nat. Commun.* **2021**, *12* (1), No. 7215.
(18) Donahue, N. M.; Drozd, G. T.; Epstein, S. A.; Presto, A. A.; Kroll, J. H. Adventures in Ozoneland: Down the Rabbit-Hole. *Phys. Chem. Chem. Phys.* **2011**, *13* (23), 10848−10857.
(19) Levy, H. Normal Atmosphere: Large Radical and Formaldehyde Concentrations Predicted. *Science* **1971**, *173* (3992), 141−143.
(20) Bender, E. Disinfecting the Air with Far-Ultraviolet Light. *Nature* **2022**, *610* (7933), S46−S47.
(21) Link, M. F.; Shore, A.; Hamadani, B. H.; Poppendieck, D. Ozone Generation from a Germicidal Ultraviolet Lamp with Peak Emission at 222 nm. *Environ. Sci. Technol. Lett.* **2023**, *10* (8), 675−679.
(22) Peng, Z.; Day, D. A.; Symonds, G. A.; Jenks, O. J.; Stark, H.; Handschy, A. V.; de Gouw, J. A.; Jimenez, J. L. Significant Production of Ozone from Germicidal UV Lights at 222 nm. *Environ. Sci. Technol. Lett.* **2023**, *10* (8), 668−674.
(23) Peng, Z.; Miller, S. L.; Jimenez, J. L. Model Evaluation of Secondary Chemistry Due to Disinfection of Indoor Air with Germicidal Ultraviolet Lamps. *Environ. Sci. Technol. Lett.* **2023**, *10* (1), 6−13.
(24) Ushio, Inc.. Care222 Technical Specification Sheet. https://www.ushio.com/files/specifications/care222-filtered-far-uv-c-excimer-lamp-module-technical-data-sheet.pdf (accessed May 02, 2023).
(25) Krechmer, J.; Lopez-Hilfiker, F.; Koss, A.; Hutterli, M.; Stoermer, C.; Deming, B.; Kimmel, J.; Warneke, C.; Holzinger, R.; Jayne, J.; Worsnop, D.; Fuhrer, K.; Gonin, M.; de Gouw, J. Evaluation of a New Reagent-Ion Source and Focusing Ion−Molecule Reactor for Use in Proton-Transfer-Reaction Mass Spectrometry. *Anal. Chem.* **2018**, *90* (20), 12011−12018.
(26) Zaytsev, A.; Breitenlechner, M.; Koss, A. R.; Lim, C. Y.; Rowe, J. C.; Kroll, J. H.; Keutsch, F. N. Using Collision-Induced Dissociation to Constrain Sensitivity of Ammonia Chemical Ionization Mass Spectrometry (NH_4^+ CIMS) to Oxygenated Volatile Organic Compounds. *Atmos. Meas. Technol.* **2019**, *12* (3), 1861−1870.
(27) DeCarlo, P. F.; Kimmel, J. R.; Trimborn, A.; Northway, M. J.; Jayne, J. T.; Aiken, A. C.; Gonin, M.; Fuhrer, K.; Horvath, T.; Docherty, K. S.; Worsnop, D. R.; Jimenez, J. L. Field-Deployable, High-Resolution, Time-of-Flight Aerosol Mass Spectrometer. *Anal. Chem.* **2006**, *78* (24), 8281−8289.
(28) Stewart, D. J.; Almabrok, S. H.; Lockhart, J. P.; Mohamed, O. M.; Nutt, D. R.; Pfrang, C.; Marston, G. The Kinetics of the Gas-Phase Reactions of Selected Monoterpenes and Cyclo-Alkenes with Ozone and the NO_3 Radical. *Atmos. Environ.* **2013**, *70*, 227−235.
(29) Aschmann, S. M.; Arey, J.; Atkinson, R. Kinetics and Products of the Reactions of OH Radicals with Cyclohexene, 1-Methyl-1-Cyclohexene, *Cis* -Cyclooctene, and *Cis* -Cyclodecene. *J. Phys. Chem. A* **2012**, *116* (38), 9507−9515.
(30) D'Anna, B.; Andresen, Ø.; Gefen, Z.; J Nielsen, C. Kinetic Study of OH and NO_3 Radical Reactions with 14 Aliphatic Aldehydes. *Phys. Chem. Chem. Phys.* **2001**, 3 (15), 3057−3063.
(31) Grøntoft, T.; Raychaudhuri, M. R. Compilation of Tables of Surface Deposition Velocities for O_3, NO_2 and SO_2 to a Range of Indoor Surfaces. *Atmos. Environ.* **2004**, *38* (4), 533−544.
(32) Saunders, S. M.; Jenkin, M. E.; Derwent, R. G.; Pilling, M. J. Protocol for the Development of the Master Chemical Mechanism, MCM v3 (Part A): Tropospheric Degradation of Non-Aromatic Volatile Organic Compounds. *Atmos. Chem. Phys.* **2003**, *3* (1), 161−180.
(33) Hansel, A.; Scholz, W.; Mentler, B.; Fischer, L.; Berndt, T. Detection of RO_2 Radicals and Other Products from Cyclohexene Ozonolysis with NH_4^+ and Acetate Chemical Ionization Mass Spectrometry. *Atmos. Environ.* **2018**, *186*, 248−255.
(34) Aschmann, S. M.; Tuazon, E. C.; Arey, J.; Atkinson, R. Products of the Gas-Phase Reaction of O_3 with Cyclohexene. *J. Phys. Chem. A* **2003**, *107* (13), 2247−2255.
(35) Barua, S.; Iyer, S.; Kumar, A.; Seal, P.; Rissanen, M. An Aldehyde as a Rapid Source of Secondary Aerosol Precursors: Theoretical and Experimental Study of Hexanal Autoxidation. *Atmos. Chem. Phys.* **2023**, *23*, 10517−10532.
(36) Singer, B. C.; Coleman, B. K.; Destaillats, H.; Hodgson, A. T.; Lunden, M. M.; Weschler, C. J.; Nazaroff, W. W. Indoor Secondary Pollutants from Cleaning Product and Air Freshener Use in the Presence of Ozone. *Atmos. Environ.* **2006**, *40* (35), 6696−6710.

(37) Wainman, T.; Zhang, J.; Weschler, C. J.; Lioy, P. J. Ozone and Limonene in Indoor Air: A Source of Submicron Particle Exposure. *Environ. Health Perspect.* **2000**, *108* (12), 1139−1145.
(38) Price, D. J.; Day, D. A.; Pagonis, D.; Stark, H.; Algrim, L. B.; Handschy, A. V.; Liu, S.; Krechmer, J. E.; Miller, S. L.; Hunter, J. F.; de Gouw, J. A.; Ziemann, P. J.; Jimenez, J. L. Budgets of Organic Carbon Composition and Oxidation in Indoor Air. *Environ. Sci. Technol.* **2019**, *53* (22), 13053−13063.
(39) Mattila, J. M.; Arata, C.; Abeleira, A.; Zhou, Y.; Wang, C.; Katz, E. F.; Goldstein, A. H.; Abbatt, J. P. D.; DeCarlo, P. F.; Vance, M. E.; Farmer, D. K. Contrasting Chemical Complexity and the Reactive Organic Carbon Budget of Indoor and Outdoor Air. *Environ. Sci. Technol.* **2022**, *56* (1), 109−118.
(40) International Commission on Non-Ionizing Radiation Protection (ICNIRP). Guidelines on Limits of Exposure to Ultraviolet Radiation of Wavelengths between 180 nm and 400 nm (Incoherent Optical Radiation). *Health Phys.* **2004**, *87* (2), 171−186.
(41) American Conference of Governmental Industrial Hygienists. *2023 Threshold Limit Values (TLVs) and Biological Exposure Indices (BEIs)*, 2023.
(42) Eadie, E.; Hiwar, W.; Fletcher, L.; Tidswell, E.; O'Mahoney, P.; Buonanno, M.; Welch, D.; Adamson, C. S.; Brenner, D. J.; Noakes, C.; Wood, K. Far-UVC (222 nm) Efficiently Inactivates an Airborne Pathogen in a Room-Sized Chamber. *Sci. Rep.* **2022**, *12* (1), No. 4373.
(43) Esvelt, K. M. *Delay, Detect, Defend: Preparing for a Future in Which Thousands Can Release New Pandemics*, The Geneva Centre for Security and Policy, 2022.
(44) ASHRAE/ANSI Standard 62.1−2022. *Ventilation and Acceptable Indoor Air Quality*, 2022.
(45) Ma, B.; Linden, Y. S.; Gundy, P. M.; Gerba, C. P.; Sobsey, M. D.; Linden, K. G. Inactivation of Coronaviruses and Phage Phi6 from Irradiation across UVC Wavelengths. *Environ. Sci. Technol. Lett.* **2021**, *8* (5), 425−430.
(46) Weschler, C. J. Ozone's Impact on Public Health: Contributions from Indoor Exposures to Ozone and Products of Ozone-Initiated Chemistry. *Environ. Health Perspect.* **2006**, *114* (10), 1489−1496.
(47) Weschler, C. J.; Shields, H. C. Production of the Hydroxyl Radical in Indoor Air. *Environ. Sci. Technol.* **1996**, *30* (11), 3250−3258.
(48) Weschler, C. J.; Shields, H. C. Measurements of the Hydroxyl Radical in a Manipulated but Realistic Indoor Environment. *Environ. Sci. Technol.* **1997**, *31* (12), 3719−3722.
(49) Carslaw, N. A New Detailed Chemical Model for Indoor Air Pollution. *Atmos. Environ.* **2007**, *41* (6), 1164−1179.
(50) Waring, M. S.; Wells, J. R. Volatile Organic Compound Conversion by Ozone, Hydroxyl Radicals, and Nitrate Radicals in Residential Indoor Air: Magnitudes and Impacts of Oxidant Sources. *Atmos. Environ.* **2015**, *106*, 382−391.
(51) Carslaw, N.; Fletcher, L.; Heard, D.; Ingham, T.; Walker, H. Significant OH Production under Surface Cleaning and Air Cleaning Conditions: Impact on Indoor Air Quality. *Indoor Air* **2017**, *27* (6), 1091−1100.
(52) Gligorovski, S.; Weschler, C. J. The Oxidative Capacity of Indoor Atmospheres. *Environ. Sci. Technol.* **2013**, *47* (24), 13905−13906.
(53) Fiorentino, E.-A.; Chen, H.; Gandolfo, A.; Lannuque, V.; Sartelet, K.; Wortham, H. Measurements and Modelling of OH and Peroxy Radicals in an Indoor Environment Under Different Light Conditions and VOC Levels. *Atmos. Environ.* **2023**, *292*, No. 119398.
(54) Mendez, M.; Amedro, D.; Blond, N.; Hauglustaine, D. A.; Blondeau, P.; Afif, C.; Fittschen, C.; Schoemaecker, C. Identification of the Major HO_x Radical Pathways in an Indoor Air Environment. *Indoor Air* **2017**, *27* (2), 434−442.
(55) Alvarez, E. G.; Amedro, D.; Afif, C.; Gligorovski, S.; Schoemaecker, C.; Fittschen, C.; Doussin, J.-F.; Wortham, H. Unexpectedly High Indoor Hydroxyl Radical Concentrations Associated with Nitrous Acid. *Proc. Natl. Acad. Sci. U.S.A.* **2013**, *110* (33), 13294−13299.
(56) Zannoni, N.; Lakey, P. S. J.; Won, Y.; Shiraiwa, M.; Rim, D.; Weschler, C. J.; Wang, N.; Ernle, L.; Li, M.; Bekö, G.; Wargocki, P.; Williams, J. The Human Oxidation Field. *Science* **2022**, *377* (6610), 1071−1077.
(57) Kowal, S. F.; Allen, S. R.; Kahan, T. F. Wavelength-Resolved Photon Fluxes of Indoor Light Sources: Implications for HO_x Production. *Environ. Sci. Technol.* **2017**, *51* (18), 10423−10430.
(58) Rosales, C. M. F.; Jiang, J.; Lahib, A.; Bottorff, B. P.; Reidy, E. K.; Kumar, V.; Tasoglou, A.; Huber, H.; Dusanter, S.; Tomas, A.; Boor, B. E.; Stevens, P. S. Chemistry and Human Exposure Implications of Secondary Organic Aerosol Production from Indoor Terpene Ozonolysis. *Sci. Adv.* **2022**, *8* (8), No. eabj9156.
(59) Reidy, E.; Bottorff, B. P.; Rosales, C. M. F.; Cardoso-Saldaña, F. J.; Arata, C.; Zhou, S.; Wang, C.; Abeleira, A.; Ruiz, L. H.; Goldstein, A. H.; Novoselac, A.; Kahan, T. F.; Abbatt, J. P. D.; Vance, M. E.; Farmer, D. K.; Stevens, P. S. Measurements of Hydroxyl Radical Concentrations during Indoor Cooking Events: Evidence of an Unmeasured Photolytic Source of Radicals. *Environ. Sci. Technol.* **2023**, *57* (2), 896−908.
(60) Wang, H.; Morrison, G. Ozone-Surface Reactions in Five Homes: Surface Reaction Probabilities, Aldehyde Yields, and Trends. *Indoor Air* **2010**, *20* (3), 224−234.

https://doi.org/10.1021/acs.est.3c05680
Environ. Sci. Technol. 2023, 57, 15990−15998